Inorganic Chemistry
Article

Inorg. Chem. **2010**, *49*, 5107–5119 **5107**
DOI: 10.1021/ic1002226

Highly Luminescent Tetradentate Bis-Cyclometalated Platinum Complexes: Design, Synthesis, Structure, Photophysics, and Electroluminescence Application[⊥]

Dileep A. K. Vezzu,[†] Joseph C. Deaton,[‡] James S. Jones,[§] Libero Bartolotti,[†] Caleb F. Harris,[†] Alfred P. Marchetti,[∥] Marina Kondakova,[‡] Robert D. Pike,[§] and Shouquan Huo*[,†]

[†]*Department of Chemistry, East Carolina University, Greenville, North Carolina 27858,* [‡]*Eastman Kodak Company, Rochester, New York 14650,* [§]*Department of Chemistry, College of William and Mary, Williamsburg, Virginia 23185, and* [∥]*Department of Chemistry, University of Rochester, Rochester, New York 14627*

Received February 4, 2010

N,*N*-Di(6-phenylpyridin-2-yl)aniline (**L1**), *N*,*N*-di(6-(2,4-difluorophenyl)pyridin-2-yl)aniline (**L2**), *N*,*N*-di(3-(pyridin-2-yl)-phenyl)aniline (**L3**), *N*,*N*-di(3-(1*H*-pyrazol-1-yl)phenyl)aniline (**L4**), *N*,*N*-di(3-(3-methyl-1*H*-pyrazol-1-yl)phenyl)aniline (**L5**), and *N*,*N*-di(3-(4-methyl-1*H*-pyrazol-1-yl)phenyl)aniline (**L6**) undergo cyclometalation to produce two types of tetradentate bis-cyclometalated platinum(II) complexes: C^N*N^C platinum complexes **1** and **2** and N^C*C^N platinum complexes **3**−**6**, respectively, where an "X^Y" (X, Y = C or N) denotes a bidentate coordination to the platinum to form a five-membered metallacycle and "X*Y" denotes a coordination to form a six-membered metallacycle. The crystal structures of **1**, **3**, and **5** were determined by the single-crystal X-ray diffraction analysis, showing distorted square-planar geometry, that is, two C^N coordination moieties are twisted. Complex **5** showed much greater distortion with largest deviation of 0.193 Å from the mean NCCNPt coordination plane, which is attributed to the steric interaction between the two 3-methyl groups on the pyrazolyl rings. Density functional theory (DFT) calculations were carried out on the ground states of **1** and **3**−**6**. The optimized geometries are consistent with the crystal structures. The highest occupied molecular orbitals (HOMOs) and lowest unoccupied molecular orbitals (LUMOs) of the molecules displayed a localized characteristic with the contribution (18−45%) of the platinum metal to the HOMOs. All complexes are emissive at ambient temperature in fluid with quantum yields of 0.14 to 0.76 in 2-methyltetrahydrofuran. The emission of the complexes covers from blue to red region with λ_{max} ranging from 474 to 613 nm. Excimer emission was observed for **1** and **2** at high concentration of the complexes. The emission lifetime at infinite dilution for **1** and **2** was determined to be 7.8 and 11.4 μs, respectively. Concentration quenching was observed for **3** and **4**, but the excimer emission was not observed. The life times for **3**−**6** were determined to be in the range of micro seconds, but those of **4**−**6** (3.4−5.7 μs) were somewhat shorter than that of **3** (7.6 μs). The highly structured emission spectra, long life times, and DFT calculations suggested that the emissive state is primarily a ^{3}LC state with metal-to-ligand charge-transfer (MLCT) admixture. The ZFS of 23 cm^{-1} for the emissive triplet state was observed directly by high resolution spectroscopy for **1** in a Shpol'skii matrix, which also suggested an emission from a triplet ligand centered (^{3}LC) state with admixture of MLCT character. Complex **1** was incorporated into an organic light-emitting diode (OLED) device as an emitter at 4 wt % in the mixed host of 4,4′,4″-*tris*(*N*-carbazolyl)triphenylamine (TCTA) and 2,2′,2″-(1,3,5-benzenetriyl)*tris*(1-phenyl-1-*H*-benzimidazole) (TPBI) and demonstrated excellent performance with maximum external quantum efficiency of 14.7% at the current density of 0.01 mA/cm^{-1}.

Introduction

Cyclometalated complexes of platinum have recently been the focus of the research for a variety of applications from catalysts to advanced materials. Cyclometalated platinum complexes have been used as oxygen sensors,[1] in the detection of cyanogen halides,[2] in cation recognition,[3] and in pH sensing.[4] They have also been used as biological labeling

[⊥] Work carried out at Eastman Kodak Company, Rochester, NY 14650, was done prior to December, 2009.

*To whom correspondence should be addressed. E-mail: huos@ecu.edu.

(1) (a) Ma, Y.-G.; Cheung, T.-C.; Che, C.-M.; Shen, J.-C. *Thin Solid Films* **1998**, *333*, 224–227. (b) Evans, R. C.; Douglas, P.; Williams, J. A. G.; Rochester, D. L. *J. Fluoresc.* **2006**, *16*, 201–6.

(2) Thomas, S. W., III; Venkatesan, K.; Muller, P.; Swager, T. M. *J. Am. Chem. Soc.* **2006**, *128*, 16641–16648.

(3) (a) Siu, P.K.-M.; Lai, S.-W.; Lu, W.; Zhu, N.; Che, C.-M. *Eur. J. Inorg. Chem.* **2003**, 2749–2752. (b) Lanoë, P.-H.; Fillaut, J.-L.; Toupet, L.; Williams, J. A. G.; Bozec, H. L.; Guerchais, V. *Chem. Commun.* **2008**, 4333–4335.

(4) (a) Wong, K.-H.; Chan, M. C.-W.; Che, C.-M. *Chem.—Eur. J.* **1999**, *5*, 2845–2849. (b) Koo, C.-K.; Ho, Y.-M.; Chow, C.-F.; Lam, M. H.-W.; Lau, T.-C.; Wong, W.-Y. *Inorg. Chem.* **2007**, *46*, 3603–3612.

Published on Web 04/28/2010

reagents,[5] photooxidation catalysts,[6] and anticancer agents.[7] More recently, the cyclometalated platinum complexes have been investigated for photogeneration of hydrogen from water.[8] In particular, the platinum complexes that emit phosphorescent light at ambient temperature have shown attractive applications in highly efficient organic light-emitting diode (OLED) devices.[9] In an OLED device, both singlet and triplet excitons are generated in about 1 to 3 ratio by charge recombination.[10] Transitions from triplet excited states to the singlet ground state are spin forbidden, therefore only the singlet excitons, that is, about 25% of total excitons generated in the OLED, can be harvested with the use of a fluorescent emitter. However, this issue can be addressed by the use of a phosphorescent emitter, which can harness both singlet and triplet excitons and maximize the internal quantum efficiency.[11] Room-temperature phosphorescence emitted from platinum complexes is attributed to the large spin−orbital coupling constant of platinum, which enables an efficient singlet−triplet intersystem crossing and makes the triplet transitions allowed. Cyclometalating ligands in the platinum complexes play an important role as they serve as a strong σ donating ligand that can induce large d orbital splitting and raise the $d_{x^2-y^2}$ to higher energy than the anti-bonding ligand π^* orbital(s), which minimizes the undesired non-radiative d-d transition and improves phosphorescence quantum efficiency. The involvement of the platinum in the electronic transitions is essential to the phosphorescent emission; therefore they are usually characterized as either MLCT (metal to ligand charge transfer) or LC (ligand centered) transitions with MLCT admixture.

There are typically two classes of cyclometalated platinum complexes that have been extensively investigated, that is, bidentate cyclometalated complexes such as *cis*-$Pt(ppy)_2$ (Hppy = 2-phenylpyridine) and (ppy)Pt(acac)[12] and tridentate cyclometalated complexes such as those derived from tridentate C^N^N (6-phenyl-2,2′-bipyridine),[13] C^N^C (2,6-diphenylpyridine),[14] and N^C^N (1,3-dipyridylbenzene)[15] ligands. Some of the complexes, particularly those based on N^C^N ligands, have shown potential as highly efficient triplet emitters in OLED devices.[16]

The photophysics of bidentate bis-cyclometalated platinum complexes has been extensively investigated.[17] However, their application to OLED devices is rather limited by their photophysical characteristics and thermal stability. For example, *cis*-$Pt(ppy)_2$ was reported to be nearly nonemissive at room temperature.[17a] On the other hand, $Pt(thpy)_2$ (Hthpy = 2-(2-thienyl)pyridine) was emissive at room temperature but unstable toward sublimation,[18] thus unsuitable for the vapor deposition process required for producing highly efficient small molecule OLED devices. The lack of room temperature phosphorescence and thermal stability is at least partially attributed to the flexibility of the molecules and the D_{2d} distortion resulting from the steric hindrance between the bidentate ligands in those bis-cyclometalated platinum complexes; therefore, the design of a more rigid structure would address those issues and improve the emission efficiency. Here we report design, synthesis, structure, and photophysical studies of highly emissive tetradentate bis-cyclometalated platinum complexes as well as their potential application as phosphorescent emitters in vapor-deposited OLED devices.[19] Platinum(II) complexes with tetradentate N_2O_2 ligands have been reported as robust and good phosphorescent emitters.[19b−d]

Results and Discussion

Design and Synthesis of the Ligands and the Complexes. One way of making the bidentate bis-cyclometalated platinum complexes such as *cis*-$Pt(ppy)_2$ more rigid is to form a tetradentate cyclometalating ligand by linking

(5) (a) Siu, P. K.-M.; Ma., D.-L.; Che, C.-M. *Chem. Commun.* **2005**, 1025–1027. (b) Botchway, S. W.; Charnley, M.; Haycock, J. W.; Parker, A. W.; Rochester, D. L.; Weinstein, J. A.; Williams, J. A. G. *Proc. Natl. Acad. Sci. U.S.A.* **2008**, *105*, 16071–16076. (c) Ma, D.-L.; Che, C.-M.; Yan, S.-C. *J. Am. Chem. Soc.* **2009**, *131*, 1835–1846. (d) Wu, P.; Wong, E.L.-M.; Ma, D.-L.; Tong, G. S.-M.; Ng, K.-M.; Che, C.-M. *Chem.—Eur. J.* **2009**, *15*, 3652–3656.

(6) Feng, K.; Zhang, R. Y.; Wu, L.-Z.; Tu, B.; Peng, M.-L.; Zhang, L.-P.; Zhao, D.; Tung, C.-H. *J. Am. Chem. Soc.* **2006**, *128*, 14685–14690.

(7) Sun, R. W.-Y.; Ma, D.-L.; Wong, E. L.-M.; Che, C.-M. *Dalton Trans.* **2007**, 4884–4892.

(8) Schneider, J.; Du, P.; Jarosz, P.; Lazarides, T.; Wang, X.; Brennessel, W. W.; Eisenberg, R. *Inorg. Chem.* **2009**, *48*, 4306–4316.

(9) For a recent review, see: Williams, J. A. G.; Develay, S. D.; Rochester, D. L.; Murhy, L. *Coord. Chem. Rev.* **2008**, *252*, 2596–2611.

(10) Baldo, M. A.; O'Brien, D. F.; Thompson, M. E.; Forrest, S. R. *Phys. Rev. B* **1999**, *60*, 14422–14428.

(11) (a) Baldo, M. A.; O'Brien, D. F.; You, Y.; Shoustikov, A.; Sibley, S.; Thompson, M. E.; Forrest, S. R. *Nature* **1998**, *395*, 151. (b) Adachi, C.; Baldo, M. A.; Forrest, S. R.; Thompson, M. E. *Appl. Phys. Lett.* **2000**, *77*, 904–906. (c) Adachi, C.; Baldo, M. A.; Thompson, M. E.; Forrest, S. R. *J. Appl. Phys.* **2001**, *90*, 5048–5051.

(12) (a) Chassot, L.; Müller, E.; von Zelewsky, A. *Inorg. Chem.* **1984**, *23*, 4249–4253. (b) Deuschel-Cornioley, C.; Luond, R.; von Zelewsky, A. *Helv. Chim. Acta* **1989**, *72*, 377–382. (c) Brooks, J.; Babayan, Y.; Lamansky, S.; Djurovich, P. I.; Tsyba, I.; Bau, R.; Thompson, M. E. *Inorg. Chem.* **2002**, *41*, 3055–3066.

(13) (a) Constable, E. C.; Henney, R. P. G.; Leese, T. A.; Tocher, D. A. *J. Chem. Soc., Chem., Commun.* **1990**, 513–515. (b) Lai, S. -W.; Chan, M. C. W.; Cheung, T.-C.; Peng, S.-M.; Che, C.-M. *Inorg. Chem.* **1999**, *38*, 4046–4055. (c) Che., C.-M.; Fu, W.-F.; Lai, S.-W.; Hou, Y.-J.; Liu, Y.-L. *Chem. Commun.* **2003**, 118–119. (d) Lu, W.; Mi, B.-X.; Chan, M. C. W.; Hui, Z.; Che, C.-M.; Zhu, N.; Lee, S. T. *J. Am. Chem. Soc.* **2004**, *126*, 4958–4971.

(14) (a) Cave, G. W. V.; Alcock, N. W.; Rourke, J. P. *Organometallics* **1999**, *18*, 1801. (b) Lu, W.; Chan, M. C. W.; Cheung, K.-K.; Che, C.-M. *Organometallics* **2001**, *20*, 2477. (c) Yam, V. W.-W.; Tang, R. P.-L.; Wong, K. M.-C.; Lu, X.-X.; Cheung, K.-K.; Zhu, N. *Chem.−Eur. J.* **2002**, *8*, 4066.

(15) (a) Cárdenas, D. J.; Echavarren, A. M.; Ramírez de Arellano, M. C. *Organometallics* **1999**, *18*, 3337–3341. (b) Song, D.; Wu, Q.; Hook, A.; Kozin, I.; Wang, S. *Organometallics* **2001**, *20*, 4683–4689. (c) Williams, J. A. G.; Beeby, A.; Davies, E. S.; Weinstein, J. A.; Wilson, C. *Inorg. Chem.* **2003**, *42*, 8609–8611. (d) Jude, H.; Bauer, J. A. K.; Connick, W. B. *Inorg. Chem.* **2004**, *43*, 725.

(16) (a) Sotoyama, W.; Satoh, T.; Sawatani, N.; Inoue, H. *Appl. Phys. Lett.* **2005**, *86*, 153505. (b) Huo, S.; Deaton, J. C.; Sowinski, A. F. U.S. Patent 7,029,766, April 18, **2006**, pp 24. (c) Kui, S. C. F.; Sham, I. H. T.; Cheung, C. C. C.; Ma, C.-W.; Yan, B.; Zhu, N.; Che, C.-M.; Fu, W. F. *Chem.—Eur. J.* **2007**, *13*, 417. (d) Cocchi, M.; Virgili, D.; Rochester, D. L.; William, J. A. G. *Adv. Funct. Mater.* **2007**, *17*, 285. (e) Cocchi, M.; Virgili, D.; Rochester, D. L.; William, J. A. G.; Kalinowski, J. *Appl. Phys. Lett.* **2007**, *90*, 163508. (f) Yan, B.-P.; Cheung, C. C. C.; Kui, S. C. F.; Roy, V. A. L.; Che, C.-M.; Xu, S. J. *Appl. Phys. Lett.* **2007**, *91*, 063508.

(17) (a) Maestri, M.; Sandrini, D.; Balzani, V.; Chassot, L.; Jolliet, P.; von Zelewsky, A. *Chem. Phys. Lett.* **1985**, *122*, 375. (b) Maestri, M.; Sandrini, D.; Balzani, V.; von Zelewsky, A.; Deuschel-Cornioley, C.; Jolliet, P. *Helv. Chim. Acta* **1988**, *71*, 1053. (c) Gianini, M.; Forster, A.; Haag, P.; von Zelewsky, A.; Stoeckli-Evans, H. *Inorg. Chem.* **1996**, *35*, 4889.

(18) Thompson, M. E.; Djurovich, P.; Lamansky, S.; Forrest, S. R.; Baldo, M. A.; Burrows, P. E. U.S. Patent, 6,830,828, December 14, **2004**, 74pp.

(19) Part of the results has been presented at the 234th ACS meeting: (a) Huo, S.; Deaton, J. C.; Kondakova, M.; Rajeswaran, M.; Giesen, D.; Lenhart, W. C. *Abstracts of Papers*, 234th National Meeting of the American Chemical Society, Boston, MA, August 19−23, 2007, IONR-911; American Chemical Society: Washington, DC, 2007; For platinum (II) complexes with tetradentate N_2O_2 ligands: (b) Che, C.-M.; Chan, S.-C.; Xiang, H.-F.; Chan, M. C. W.; Liu, Y.; Wang, Y. *Chem. Commun.* **2004**, 1484–1485. (c) Lin, Y. Y.; Chan, S.-C.; Chan, M. C. W.; Hou, Y.-J.; Zhu, N.; Che, C.-M.; Liu, Y.; Wang, Y. *Chem. −Eur. J.* **2003**, *9*, 1264–1272. (d) Che, C.-M.; Kwok, C.-C.; Lai, S.-W.; Rausch, A. F.; Finkenzeller, W. J.; Zhu, N.; Yersin, H. *Chem.−Eur. J.* **2010**, *16*, 233–247.

Scheme 1. Tetradentate Cyclometalating Ligands with Different Coordination Geometries

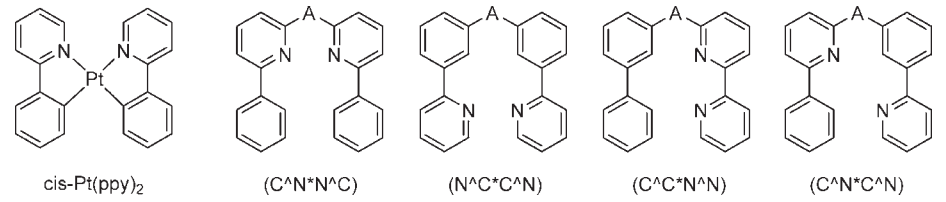

Scheme 2. Synthesis of Tetradentate Bis-cyclometalated Platinum Complexes[a]

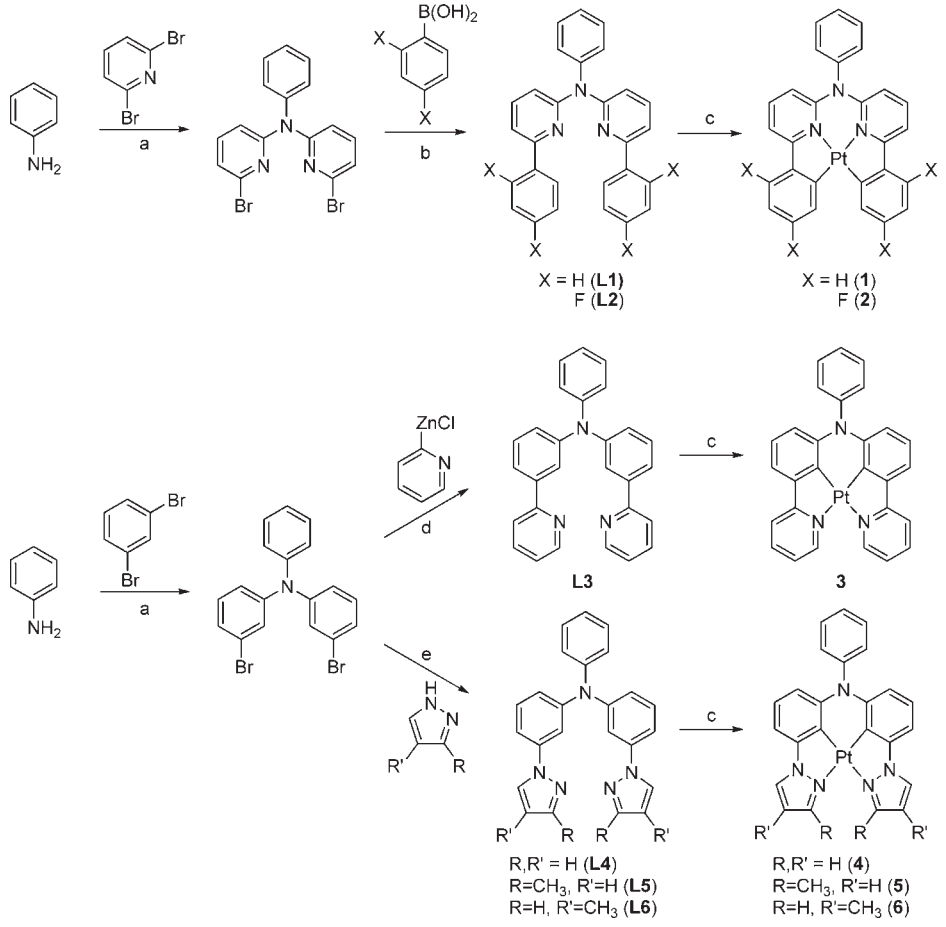

[a] Reagents and conditions: (a) $Pd(dba)_2$ (2%), DPPF (2%), NaO^tBu (1.2 equiv), toluene, reflux. (b) $Pd(OAc)_2$ (2%), PPh_3 (8%), DME, 2 M Na_2CO_3 (aq), reflux. (c) K_2PtCl_4 (1 equiv), AcOH, reflux. (d) $Pd(PPh_3)_4$ (5%), THF, 50 °C. (e) CuI (5%), *trans*-*N*,*N*′-dimethylcyclohexanediamine (20%), toluene, reflux.

the two bidentate cyclometalating ligands together. The tetradentate ligands can coordinate to platinum through two carbon−platinum covalent bonds and two nitrogen−platinum coordinative bonds to form a bis-cyclometalated complex. It can be readily envisaged that such tetradentate cyclometalating ligands can have different coordination geometries, that is, C^N*N^C, N^C*C^N, C^C*N^N, and C^N*C^N, as shown in Scheme 1, where an "X^Y" (X, Y = C or N) denotes a bidentate coordination to the platinum to form a five-membered metallacycle and "X*Y" denotes a coordination to the platinum to form a six-membered metallacycle. In this paper we will report on the first two types of complexes (C^N*N^C)Pt and (N^C*C^N)Pt.

Although there are many ways of linking two bidentate cyclometalating ligands to form a tetradentate ligand, we have chosen an amine linker in this study, mainly because of the high modularity in ligand design and the simplicity in ligand syntheses. As demonstrated in Scheme 2, the synthesis of the tetradentate C^N*N^C and N^C*C^N ligands **L1**−**L6** can be efficiently achieved by using the combination of the palladium-catalyzed C−C and palladium or copper-catalyzed C−N bond cross coupling reactions.

The C^N*N^C ligands **L1** and **L2** was prepared by two steps of Pd-catalyzed cross-coupling reactions. The C−N coupling[20] of aniline with excess amounts of 2,6-dibromopyridine produced intermediate dibromide as the major product, which was readily separated from oligomeric byproducts by column chromatography. The tetradentate cyclometalating ligands **L1** and **L2** were then prepared in

(20) Yang, J.-S.; Lin, Y.-H.; Yang, C.-S. *Org. Lett.* **2002**, *4*, 777.

Scheme 3. Undesired Cyclometalation of NCCN Ligand

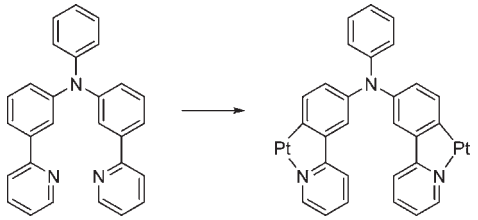

good yields by the Pd-catalyzed C−C cross coupling[21] of the dibromide with phenylboronic acid and 2,4-difluorophenylboronic acid, respectively. The N^C*C^N ligand **L3**−**L6** were prepared similarly using 1,3-dibromobenzene as one of the starting materials except for the second step. The preparation of **L3** involved the Negishi coupling[22] of the dibromide intermediate with the 2-pyridylzinc halide reagent generated in situ from the treatment of 2-bromopyridine with *n*-butyllithium followed by transmetalation with $ZnCl_2$, while **L4**−**L6** were prepared using a Cu(I)-catalyzed carbon−nitrogen bond formation protocol developed by Buchwald et al.[23] It is known that bidentate bis-cyclometalated platinum complex *cis*-$Pt(ppy)_2$ could not be prepared by direct cyclometalation reactions because the direct metalation with K_2PtCl_4 produced only chloride-bridged dinuclear monocyclometalated complexes. Rather, it was prepared from the transmetalation of $Pt(SEt)_2Cl_2$ with the corresponding organolithium reagents.[12a] In contrast, the reaction of the ligands **L1** and **L2** with K_2PtCl_4 in acetic acid gave the desired bis-cyclometalated platinum complexes **1** and **2** in high yields, which may be attributed to the fact of the second C−Pt bond formation being an intramolecular process that is generally considered to be more favorable than an intermolecular reaction. Complexes **3**−**6** were prepared similarly. The yields of **3**−**6** were significantly lower than those of **1** and **2**. This can be attributed to the side reactions associated with the cycloplatination occurring at unwanted sites as shown in Scheme 3, which may also produce an oligomeric complex. The complexes were easily purified by column chromatography and **1** was further purified by sublimation for OLED device fabrications. All new compounds were characterized by ^1H and ^{13}C NMR, MS, and satisfactory elemental analysis.

X-ray Crystal Structure. The molecular structure of **1**, **3**, and **5** were determined by single-crystal X-ray diffraction analysis, which confirmed the tetradentate coordination structure (Figure 1). The selected bond lengths and angles are listed in Table 2. The nonplanarity of the platinum coordination of the complexes is shown in Supporting Information, Figure S1. For complexes **1** and **3**, the two phenylpyridine rings are twisted probably because of the steric interaction of the two rings in the open end (tail) of the tetradentate complexes. The complexes have a slightly twisted planar geometry around the platinum coordination center with the largest deviation of 0.083 and 0.101 Å from the NCCNPt coordination plane for **1** and **3**, respectively. It is interesting to note that the

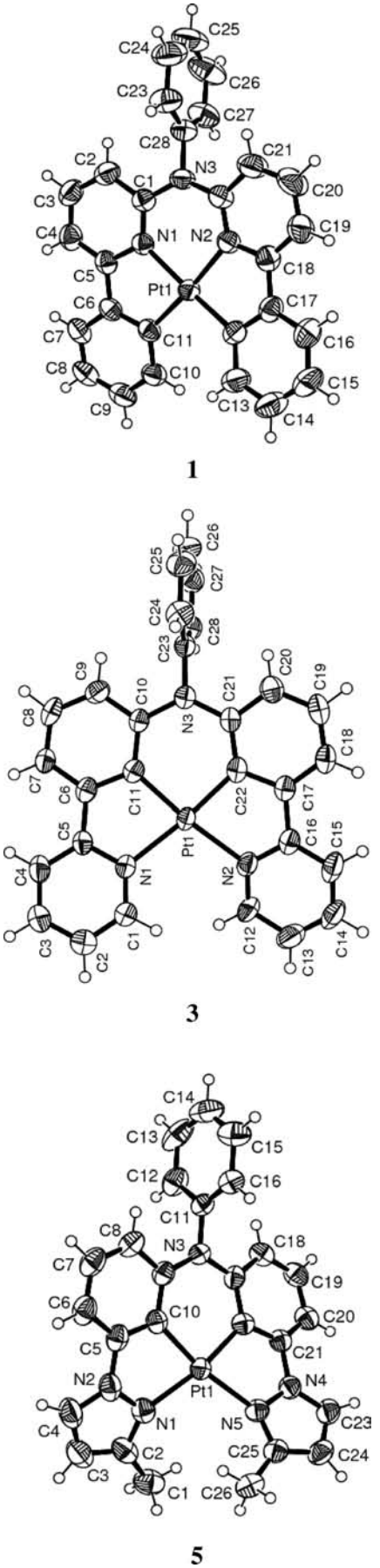

Figure 1. ORTEP drawing of molecular structure of **1**, **3**, and **5**.

(21) Lohse, O.; Thevenin, P.; Waldvogel, E. *Synlett* **1999**, 45.
(22) (a) Smith, A. P.; Savage, S. A.; Love, J. C.; Fraser, C. L. *Org. Synth.* **2002**, *78*, 51–62. (b) Alami, M.; Peyrat, J.-F.; Belachmi, L.; Brion, J.-D. *Eur. J. Org. Chem.* **2001**, 4207–4212.
(23) Antilla, J. C.; Baskin, J. M.; Barder, T.; Buchwald, S. L. *J. Org. Chem.* **2004**, *69*, 5578–5587.

Table 1. Crystal Data and Structure Refinement Details for **1**, **3**·1/3CH_2Cl_2, and **5**

	1	(3 × **3**)·CH_2Cl_2	**5**
empirical formula	$C_{28}H_{19}N_3Pt$	$C_{85}H_{59}Cl_2N_9Pt_3$	$C_{26}H_{21}N_5Pt$
formula weight	592.55	1862.58	598.57
temperature, K	296(2)	100(2)	296(2)
wavelength, Å	1.54178	1.54178	1.54178
crystal system	monoclinic	triclinic	monoclinic
space group	$P2_1/c$	$P\bar{1}$	$P2_1/c$
a, Å	13.09670(10)	11.3262(11)	7.75100(10)
b, Å	15.123492)	15.7878(14)	28.5715(4)
c, Å	11.24900(10)	20.0657(18)	10.22690(10)
α, deg	90	81.958(5)	90
β, deg	108.9899(4)	83.676(5)	106.1765(4)
γ, deg	90	83.412(6)	90
volume, Å^3	2106.79(4)	3513.1(6)	2175.16(5)
Z	4	2	4
density (calculated), Mg/m^3	1.868	1.761	12.250
absorption coefficient, mm^{-1}	12.616	12.064	12.250
F(000)	1144	1800	1160
crystal size, mm	0.40 × 0.19 × 0.18	0.68 × 0.61 × 0.05	0.42 × 0.22 × 0.19
θ range for data collection, deg	3.57 to 66.98	2.23 to 67.00	3.09 to 66.99
limiting indices	$-15 \le h \le 15$	$-12 \le h \le 13$	$-9 \le h \le 9$
	$-17 \le k \le 18$	$-18 \le k \le 18$	$-29 \le k \le 33$
	$-13 \le l \le 13$	$-23 \le l \le 23$	$-12 \le l \le 12$
reflections collected	22540	56175	23476
independent reflections (R_{int})	3584 (0.0295)	12144 (0.0535)	3797 (0.0351)
completeness to $\theta = 67.00°$	95.5%	96.9%	98.1%
absorption correction	numerical	numerical	numerical
max. and min transmission	0.2136 and 0.0811	0.5619 and 0.0450	0.2008 and 0.0787
refinement method	full-matrix least-squares on F^2	full-matrix least-squares on F^2	full-matrix least-squares on F^2
data/restraints/parameters	3584/0/290	12144/0/887	3797/0/292
goodness-of-fit on F^2	0.984	1.037	1.050
final *R* indices [$I > 2\sigma(I)$]	R1 = 0.0157, wR2 = 0.0423	R1 = 0.0530, wR2 = 0.1512	R1 = 0.0230, wR2 = 0.0635
R indices (all data)	R1 = 0.0172, wR2 = 0.0436	R1 = 0.0572, wR2 = 0.1588	R1 = 0.0237, wR2 = 0.0641
largest diff. peak and hole, e Å^{-3}	0.397 and −0.334	2.610 and −2.792	1.123 and −0.642

Table 2. Selected Bond Lengths (Å) and Angles (deg) for Compound **1**, **3**, and **5**

complex **1**		complex **3**		complex **5**	
Pt(1)−C(11)	2.000 (3)	Pt(1)−C(11)	1.960(7)	Pt(1)−C(22)	1.955(4)
Pt(1)−C(12)	2.007(3)	Pt(1)−C(22)	1.959(8)	Pt(1)−C(10)	1.956(4)
Pt(1)−N(1)	2.051(2)	Pt(1)−N(1)	2.125(7)	Pt(1)−N(5)	2.093(3)
Pt(1)−N(2)	2.050(2)	Pt(1)−N(2)	2.130(6)	Pt(1)−N(1)	2.097(3)
C(11)−Pt(1)−C(12)	103.86(11)	C(22)−Pt(1)−C(11)	93.6(3)	C(22)−Pt(1)−C(10)	92.34(16)
C(11)−Pt(1)−N(2)	173.77(9)	C(22)−Pt(1)−N(1)	170.7(3)	C(22)−Pt(1)−N(5)	80.63(15)
C(12)−Pt(1)−N(2)	82.02(10)	C(11)−Pt(1)−N(1)	80.7(3)	C(10)−Pt(1)−N(5)	166.99(14)
C(11)−Pt(1)−N(1)	81.85(10)	C(22)−Pt(1)−N(2)	81.0(3)	C(22)−Pt(1)−N(1)	167.12(14)
C(12)−Pt(1)−N(2)	171.75(10)	C(11)−Pt(1)−N(2)	173.8(3)	C(10)−Pt(1)−N(1)	80.29(15)
N(1)−Pt(1)−N(2)	92.52(8)	N(1)−Pt(1)−N(2)	105.1(2)	N(5)−Pt(1)−N(1)	108.54(13)
C(1)−N(3)−C(22)	131.4(2)	C(21)−N(3)−C(10)	126.3(6)	C(9)−N(3)−C(17)	126.6(3)
C(1)−N(3)−C(28)	114.9(2)	C(21)−N(3)−C(23)	117.0(6)	C(9)−N(3)−C(11)	117.1(3)
C(22)−N(3)−C(28)	113.7(2)	C(10)−N(3)−C(23)	116.7(6)	C(17)−N(3)−C(11)	116.2(3)

unit cell of the complex **3** contains three independent molecules with two being essentially identical, but the third one being nearly flat with the largest deviation of only 0.023 Å from the coordination plane (Supporting Information, Figure S1, **3a**). The head-to-tail stacking of molecules in the crystal packing of complex **1** suggests a weak $\pi-\pi$ stacking, if any, since the distance between two adjacent molecules is about 4.0 Å. There is no Pt−Pt interaction shown in the crystal packing of all three complexes. The N-phenyl ring is nearly perpendicular to the coordination square plane. Complex **5** has a much more severely distorted square planar geometry compared to **1** and **3** (Supporting Information, Figure S1). To minimize the steric interaction of the two methyl groups and to accommodate the square-planar geometry of the Pt(II) complex, the pyrazolyl rings are not only twisted but also bent relative to the phenyl ring that is connected to it through the C−N bond. The largest deviation from the NCCNPt coordination plane is 0.193 Å.

There are small but distinct differences in the lengths of the C−Pt and N−Pt bonds in the structures of these complexes. In complex **1** the average of the Pt−C bond lengths (2.004(5) Å) is very close to that reported for *cis*-Pt(ppy)$_2$ (1.993(13) Å), while the average of the Pt−N bonds (2.051(1) Å) is somewhat shorter than that in *cis*-Pt(ppy)$_2$ (2.127(2) Å). On the other hand, the average Pt−C bond length (1.960(1) Å) in complex **3** is slightly shorter than that reported for *cis*-Pt(ppy)$_2$, while the average Pt−N bond length (2.128(4) Å) is nearly identical to that in *cis*-Pt(ppy)$_2$. The corresponding bond lengths for **5** are similar to those of **3**. The relative shorter Pt−N bonds in **1** and Pt−C bond in **3** may be attributed to the formation of an energetically favorable six-membered

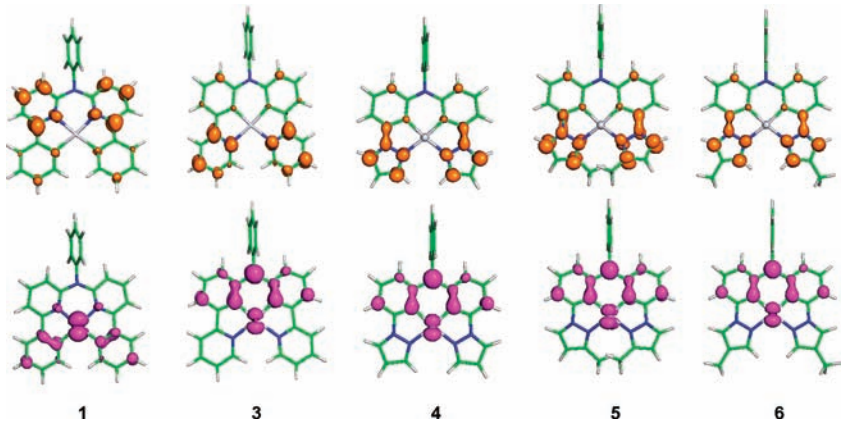

Figure 2. Density functional theory calculation (DFT) of orbit density for the HOMOs (bottom) and LUMOs (top) of **1** and **3**−**6**.

metallacycle in the tetradentate platinum complex, that is, less strained geometry when compared to other small or medium sized rings except for the five-membered ring. In addition, the electron delocalization within the metallacycle may be also responsible for the stronger Pt−N bonds in **1** and Pt−C bonds in **3**. The fact that the endo amino nitrogen−carbon bonds are shorter than the exo nitrogen−carbon in **1** and **3** is indicative of an extended conjugation through the amino nitrogen. In addition, the nitrogen adopts a planar geometry (a sum of 360 deg of the three CNC angles around the nitrogen) rather than a normal trigonal pyramidal geometry, indicating the feature of a sp^2 hybridized N for extended conjugation. The longer Pt−N bond (2.128(4) Å) in **3** relative to the Pt−C bond (2.004(5) Å) in **1** and the shorter Pt−C bond (1.960(1) Å) in **3** relative to the Pt−N bond (2.051(1) Å) in **1** may be responsible for the presence of the flat molecule in the crystal packing of **3** because the open end is more open; thus, the steric effect in **3** is less significant.

All three twisted structures have approximately C_2 symmetry with deviation from the tertiary N that leans slightly toward one side of the coordination plane, indicating that they are chiral. However, the isomerization between the two enantiomers may be too fast for them to be isolated under normal conditions. The presence of the flat structure in the crystals of **3** further indicates a free interconversion of two enantiomers. The steric hindrance between the two methyl groups in **5** may restrict such isomerization, and the complex might be resolvable.

DFT Calculations. Density functional theory (DFT) calculations were performed on complexes **1**, **3**, **4**, **5**, and **6**. The quantum mechanical computer software program G03 and the B3LYP[24,25] exchange-correlation functional were used to perform all calculations. The DEF2_TZVP basis set[26] was used for platinum, while the cc-pvdz basis set[27] was used for all other atoms. The optimized ground state geometries of **1**, **3**, and **5** compare satisfactorily to those determined by X-ray crystallography. The crystal structures of **4** and **6** were not determined; however, the optimized geometries of **4**, **5**, and **6** provide a clear comparison, showing severe distortion of the square planar coordination of the platinum complex **5** as compared to **4** and **6** because of the steric interaction of the two 3-methyl groups (Supporting Information, Figure S2).

Table 3. Calculated Energies (eV) and Energy Gaps of HOMO and LUMO Orbitals of Complexes

complex	**1**	**3**	**4**	**5**	**6**
LUMO	−1.70	−1.78	−1.31	−1.14	−1.22
HOMO	−5.27	−4.56	−4.64	−4.57	−4.55
ΔE	3.57	2.78	3.33	3.43	3.33

The orbital densities of the highest occupied molecular orbitals (HOMOs) and lowest unoccupied molecular orbitals (LUMOs) are shown in Figure 2. The composition of the frontier molecular orbitals has been very useful to interpreting the nature of the excited states and the substituent effect on the photophysical properties of platinum complexes.[28] From the composition of the HOMOs and LUMOs of the complexes, it was estimated that the platinum metal makes about a 45% contribution to the HOMO of **1** and 17−18% contribution to the HOMOs of **3**−**6**. Notably, the triarylamino nitrogen is the major contributor to the HOMOs of **3**−**6**, accounting for about 24−25%. The rest of the HOMO orbital density is localized in the phenyl rings that are connected to the pyridyl or pyrazolyl ring. The LUMOs for **1** and **3**−**6** are largely localized in the pyridyl or pyrazolyl rings with small contributions from the phenyl rings. It is interesting to note that 3- and 5-carbons in the pyrazolyl rings contribute significantly to the LUMOs of the complexes **4**, **5**, and **6** while there is essentially no contribution from the 4-carbon atom. Both HOMO and LUMO orbital densities have π symmetry. The calculated energies of the HOMOs and the LUMOs and the energy gaps are listed in Table 3. The HOMOs of **3**−**6** are significantly higher than that of **1**, reflecting the electron-donating effect of the amino nitrogen atom that contributes significantly to the HOMOs of **3**−**6** as mentioned above. The LUMO energies of **4**−**6** are much higher than that of **1**, while **3** has similar LUMO energy to that of **1**, which is consistent with the poorer electron acceptability of the pyrazolyl ring compared to the pyridine ring.[29]

Photophysical Properties. The photophysical data for all complexes are summarized in Table 4.

(24) Becke, A. D. *J. Chem. Phys.* **1993**, *98*, 5648.
(25) Lee, C.; Yang, W.; Parr, R. G. *Phys. Rev. B.* **1988**, *37*, 785.
(26) Weigend, F.; Ahlrichs, R. *Phys. Chem. Chem. Phys.* **2005**, *7*, 3297.
(27) Dunning, T. H. *J. Chem. Phys.* **1989**, *90*, 1007.
(28) Yersin, H.; Donges, D. *Top. Curr. Chem.* **2001**, *214*, 81.
(29) Develay, S.; Blackburn, O.; Thompson, A. L.; Williams, J. A. W. *Inorg. Chem.* **2008**, *47*, 11129–11142.

Table 4. Photophysical Data of Complexes **1**−**6**.[a]

complex	λ_{abs}/nm (ε/M^{-1} cm^{-1})	λ_{em}/nm (298 K)	λ_{em}/nm (solid state)	λ_{em}/nm (77 K)	τ/μs	Φ[d]
1	324 (25229), 342 (26272), 384 (4903), 407 (5969)	512, 548	514, 551,595	501, 539	7.6[b]	0.74(0.03)
2	268 (29196), 329 (18970), 387 (3891)	488, 523	541, 583	481, 517	11.4[b]	0.75(0.01)
3	274 (28533), 324 (17411), 338 (17435), 409 (9656), 507(1350)	613	741, 782	594, 637	7.6[b]	0.14(<0.01)
4	302 (34401), 335 (16243), 351 (28521), 370 (8493), 421 (3367), 442 (2880)	484, 512	509	477, 510	4.9[b]	0.56(<0.01)
5	304 (21396), 334 (10307), 348 (13294), 365 (5021), 408 (1656), 428 (1401)	474	467, 488, 540	462, 491	3.4[c]	0.37(<0.01)
6	307 (28076), 342 (10328), 357 (18193), 376 (4722), 428 (1835), 451 (1560)	486, 516	491, 517, 554	481, 513	5.7[c]	0.63(<0.01)

[a] All measurement were carried out in a solution of 2-methyltetrahydrofuran, The excitation wavelength of 350 nm was used for all compounds except for **3** where an excitation of 421 nm was used. Solid state emissions were measured with pure powder samples. [b] Emission lifetime at infinite dilution extrapolated from the Stern−Volmer expression. [c] Average of three measurements. [d] Quinine sulfate solution in 0.1 N H_2SO_4 (Φ 0.55) was used as a reference. The data in parentheses are the values measured in aerated solutions.

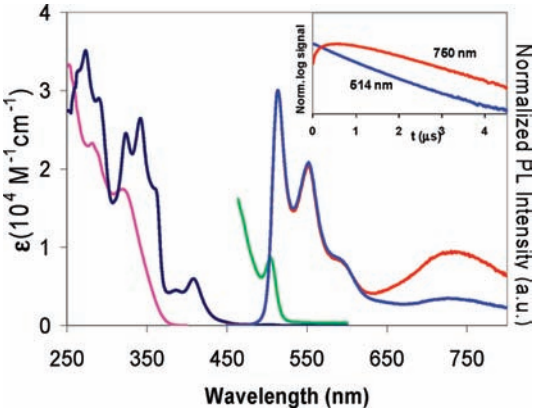

Figure 3. Absorption (**L1**: pink; **1**: black), lowest energy absorption (**1**, green), and normalized emission (**1**: blue 5.13×10^{-5} M; red 1.54×10^{-4} M) spectra (365 nm excitation) and phosphorescence decay of **1** (inset, 4.62×10^{-4} M) in 2-MeTHF at room temperature.

C^N*N^C Platinum Complexes 1 and 2. The absorption spectra of **L1** and **1** are shown in Figure 3. The emission spectra of **1** at two concentrations are shown in Figure 3 and normalized to the main peak at 514 nm. Emission decay curves of **1** at two wavelengths are shown in the inset of Figure 3. Overlapping absorption bands from 250 to 360 nm may be assigned as dominantly ligand $^1\pi-\pi^*$ transitions in view of their high extinction coefficient (17,000 to 35,000 M^{-1} cm^{-1}) and similar energies to the free ligand (**L1**) absorption bands. A band at 408 nm is significantly lower in energy than the free ligand absorptions and has extinction (5964 M^{-1} cm^{-1}) more typical of ^{1}MLCT transitions. When the absorbance was measured in a long path length cell on an expanded scale, a weak band at 504 nm was found. The low extinction of this band (83 M^{-1} cm^{-1}) suggests a transition to the triplet excited state enabled by spin−orbit coupling. The weak band at 504 nm appears to coincide with the high energy origin of the intense green emission observed at 514 nm in solution. The presence of a weak band at 504 nm in the excitation spectrum of **1** (Supporting Information, Figure S7) further supports the assignment of the triplet excited state. The quantum yield of dilute, deoxygenated solution of **1** in 2-methyltetrahydrofuran was found to be 0.74, which is among the highest reported for cyclometalated platinum complexes. When the emission of a concentration series of **1** was recorded, a broad emission at longer wavelength grew at the expense of the first emission band at 514 nm and its associated vibronic sideband (548 nm) as the concentration increased. Being the dominant emission in dilute solution, the 514 nm band may be attributed to the monomer complex emission. The long wavelength band may be attributed to the excimer[30,31] rather than aggregation of ground state molecules since the absorption of the complex was found to follow Beer's law in the concentration range used in the experiment. Excitation spectra registered at emission wavelengths of 514 and 710 nm, respectively, are identical, indicating that the emissions arise from the same ground state species. These assignments were further supported by following the time evolution of the emission bands (inset Figure 3) in which the monomer was observed to follow a single exponential decay, while the excimer emission initially increased after the excitation pulse and subsequently decayed. The observed decay rate followed a linear dependence upon concentration (Supporting Information, Figure S3) since the monomer emission was quenched as a result of excimer formation. The observed decay rate of the monomer was fit to a Stern−Volmer equation (eq 1),[31] where k_q is the self-quenching (excimer formation) rate constant, [Pt] is the concentration of the platinum complex, and k_0 is the decay rate for the monomer complex.

$$k_{obs} = k_q[Pt] + k_0 \quad (1)$$

The self-quenching rate constant k_q was 3.8×10^9 $M^{-1}sec^{-1}$, well within the range reported for other emissive platinum complexes.[31] The monomer emission lifetime ($1/k_0$) was found to be 7.8 μs, which is consistent with the emission from a $^3\pi-\pi^*$ state with MLCT admixture. The mixed state is also supported by the DFT calculation, which showed a contribution to the HOMO of **1** from both platinum and the ligand. The localized HOMO and LUMO also suggest an intraligand charge transfer (ILCT) characteristic of the excited states.

The spectral properties of **2** are broadly similar to those of **1**, except shifted to higher energy resulting from the electron-withdrawing effect of the fluorine substituents (Figure 4). The weak, lowest energy absorption was found at 480 nm (48 M^{-1} cm^{-1}) and the first more intense absorption at 387 nm (3891 M^{-1} cm^{-1}). The quantum yield of **2** in a deoxygenated solution of 2-methyltetrahydrofuran was determined to be 0.75. An observed decay time of 11.4 μs was determined for the monomer emission at infinite dilu-

(30) (a) Ma, B.; Djurovich, P. I.; Thompson, M. E. *Coord. Chem. Rev.* **2005**, *249*, 1501–1510. (b) Farley, S. J.; Rochester, D. L.; Thompson, A. L.; Howard, J. A. K.; Williams, J. A. G. *Inorg. Chem.* **2005**, *44*, 9690–9703.
(31) (a) Connick, W. B.; Gray, H. B. *J. Am. Chem. Soc.* **1997**, *119*, 11620. (b) Connick, W. B.; Geiger, D.; Eisenberg, R. *Inorg. Chem.* **1999**, *38*, 3264.

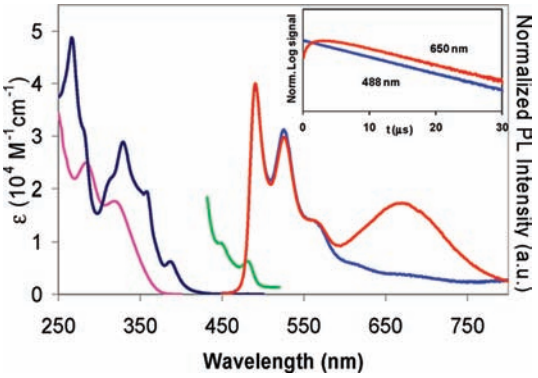

Figure 4. Absorption (**L2**: pink; **2**: black), lowest energy absorption (**2**, green), and normalized emission (**2**: blue 3.84×10^{-6} M; red 3.08×10^{-5} M) spectra (365 nm excitation) and phosphorescence decay of **2** (inset, 3.08×10^{-5} M) in 2-MeTHF at room temperature.

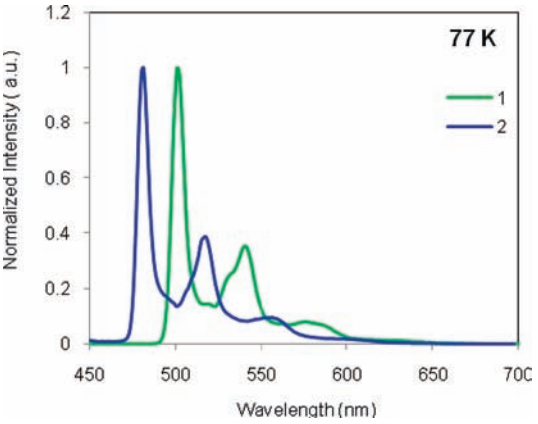

Figure 5. 77 K emission spectra of **1** and **2** in 2-methyltetrahydrofuran.

tion extrapolated from the Stern−Volmer plot (Supporting Information, Figure S4). The k_q (2.8×10^9 $M^{-1}sec^{-1}$) was similar to that for **1**. The emission of both complexes **1** and **2** sharpened at 77 K (Figure 5) and displayed vibronic progression of 1407 and 1447 cm^{-1}, respectively. The emission spectra of **1** and **2** in pure solid were recorded (Supporting Information, Figure S9), and they resemble those in solution except for the red shift. The red-shifted emission may be due to ground state intermolecular interactions in pure solid state rather than the excimer formation as observed in the solution at higher concentration, since both the emission energy and band shape are quite different from those of the excimer emission.

High resolution emission spectra were obtained for **1** in a Shpol'skii matrix of *n*-octane. As indicated in Figure 6, the spectrum at 8 K comprises (0,0) origin emission lines from several distinct sites in the matrix overtop a broad background of inhomogeneously broadened emission. At longer wavelengths, there are vibrational satellites that are relatively low in intensity relative to the more intense site origin lines. At 2 K, a new set of vibrational satellites grow in (site origins at 2 K not shown for clarity). The origin region around site B is shown on an expanded scale in Figure 7. At 40 K, there is a very weak feature at 510.94 nm, and two more intense lines at 511.82 and 512.24 nm. At 2 K, the line at 511.82 nm has lost intensity relative to the 512.24 nm line. Application of a magnetic field at 2 K causes a new line at 512.42 nm to gain

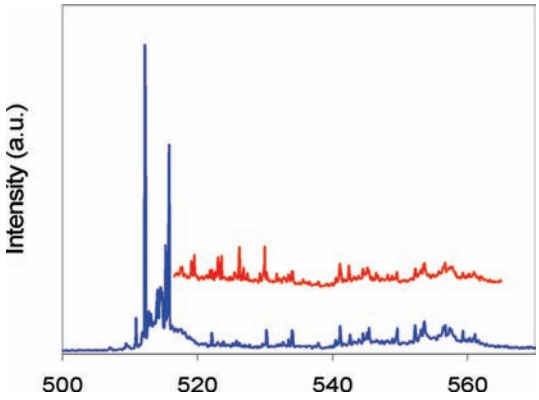

Figure 6. Emission of **1** in Shpol'skii Matrix (*n*-octane). Blue: 8 K; red: vibrational satellites at 2 K. Excitation was at 365 nm using cw Ar ion laser.

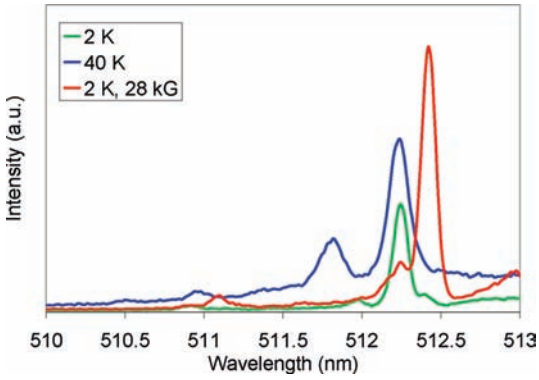

Figure 7. High-Resolution Spectra of **1** in Shpol'skii Matrix in the region of site A and site B. Blue, 40 K and zero field; green, 2 K and zero field; red, 2 K and 28 kG. Excitation was at 365 nm using cw Ar ion laser.

intensity, which was not observable in zero field. This line is more highly forbidden than the others in zero field, but under the influence of the magnetic field it gains intensity by mixing another, more allowed state. This behavior has been well documented for the lowest triplet sublevel of a number of other Pt(II) complexes.[28,32] Therefore, the 512.42 nm line is assigned by analogy as the lowest energy triplet sublevel, the 512.24 nm line as the middle, and the 511.82 nm line that was thermally depopulated as the highest energy triplet sublevel for site B. The total zero field splitting between the highest and lowest triplet sublevels is thus found to be 23 cm^{-1}, while the spacing between the middle and lowest sublevels is 7 cm^{-1}. The weak peak at 510.94 nm and the one at 511.1 nm that grew in at high field are attributed to a different site (A). The highest sublevel for this site was too weak to detect with confidence, but might be the little bump at 510.5 nm, giving a ZFS for site A of 23 cm^{-1} between highest and lowest sublevels, and 6 cm^{-1} between middle and lowest. The ZFS values found for **1** are within the range of values found for bis(C^N)-cyclometalated Pt complexes such as $Pt(ppy)_2$ (32 cm^{-1}) and $Pt(thpy)_2$ (16 cm^{-1}).[28,32a] A precise interpretation of the difference in ZFS between **1** and $Pt(ppy)_2$ cannot easily be made because it is also known that guest−host interactions can

(32) (a) Strasser, J.; Homeier, H. H. H.; Yersin, H. *Chem.. Phys.* **2000**, *255*, 301. (b) Rausch, A. F.; Murphy, L.; Williams, J. A. G.; Yersin, H. *Inorg. Chem.* **2009**, *48*, 11407–11414.

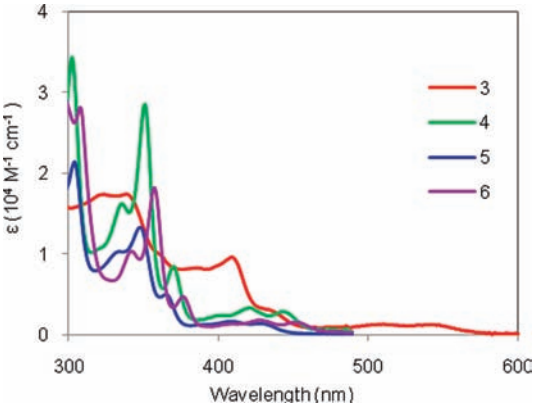

Figure 8. Absorption spectra of **3**−**6** measured in 2-methyltetrahedrofuran at room temperature.

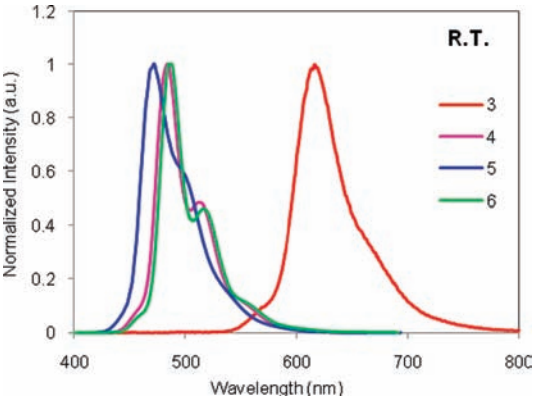

Figure 9. Room temperature emission spectra of **3**−**6** in 2-methyltetrahydrofuran.

influence the value of ZFS and may differ from site to site, even in the same host.[33]

The behavior of the vibrational satellites may be understood by analogy to that of numerous other Pt complexes that have been thoroughly studied by Yersin and coworkers.[28,32b] Because the electronic origins of the middle and upper sublevels of the triplet state were found to be relatively allowed in zero magnetic field, the vibrational satellites observed at 8 K (Figure 6), also in zero field, should be the totally symmetric, Franck−Condon modes of the complex. At 2 K, a new set of vibrational satellites grew in that must be associated with the lowest sublevel as it dominates the Boltzman distribution at 2 K. Because the electronic origin of the lowest sublevel was found to be more highly forbidden at 2 K in zero field, it is concluded that the new vibrational satellites observed at 2 K result from a spin-vibronic intensity-gaining mechanism for the lowest sublevel, and that these satellites are therefore unsymmetrical, Herzberg−Teller modes. A preliminary analysis of the totally symmetric satellite intensities relative to the respective electronic origin reveals that they have a Huang−Rhys parameters less than 0.1, indicating little geometry change between the ground and excited state. Analogous observations were recently reported for a tridentate N^C^N−Pt complex and were ascribed to the rigidity imposed by the multidentate ligand.[32b]

(33) Rausch, A. F.; Thompson, M. E.; Yersin, H. *J. Phys. Chem. A* **2009**, *113*, 5927.

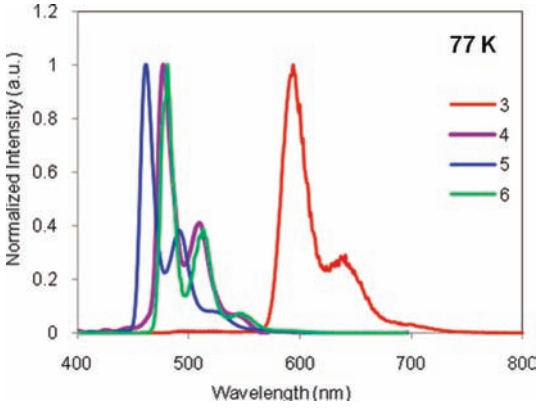

Figure 10. 77 K emission spectra for **3**−**6** in 2-methyltetrahydrofuran.

N^C*C^N Platinum Complexes 3−6. The absorption spectra and emission spectra of **3**−**6** are shown in Figure 8 and 9, respectively. These complexes displayed very similar absorption spectra except for red-shifted absorptions of **3**. As in the absorption spectra of **1** and **2**, the higher energy strong absorption bands can be assigned to ligand $^1\pi-\pi^*$ transitions. However, there are a series of relatively weak low-energy absorptions (380−470 nm for **4**−**6** and 490−570 nm for **3**) that are markedly different from those of complexes **1** and **2**. These bands have an extinction coefficient between 2000 and 4000 M^{-1} cm^{-1}, within the range for a charge transfer band. They may be assigned as either MLCT, ILCT, or mixed charge transfer (MMLLCT) transitions. The lowest energy absorptions were tentatively assigned as MMLLCT transitions, that is, a mixed d-π^* (Pt), p-π^* (the amino nitrogen), and $\pi-\pi^*$ charge transfer transition. The assignment of p-π^* transitions is based on the calculated HOMO character of these complexes which shows significant contribution from the $2p_z$ orbital of the amino nitrogen. It should be mentioned that the moderate solvent effect (10−15 nm hypsochromic shifts from toluene to acetonitrile) was observed for the low energy charge transfer absorption bands for compounds **1**, and **4**−**6**, while the effect for compound **3** appears somewhat larger (19−26 nm) (Supporting Information, Tables S2−S6). The solvent effect for **2** was not examined because of its poor solubility. The moderate effect might be due to the twisted geometry of the molecules and the dipole moment change induced by the charge transfer being moderate. The weak, lowest energy absorptions observed for **1** and **2** were not detected for the complexes **3**−**6**.

Complexes **3**−**6** emitted intensely at room temperature in a solution of 2-methyltetrahydrofuran with quantum yields of 0.14, 0.56, 0.37, and 0.63, respectively. The order of the emission energy is consistent with the HOMO−LUMO gaps calculated for **3**−**6**. Complex **3** emitted red light with λ_{max} of 613 nm. When replacing the pyridine ring in complex **3** with a pyrazolyl ring the emission was shifted to 484 nm (complex **4**), which is consistent with the poorer electron accepting ability of the pyrazolyl ring. Introduction of a methyl group to the 4-position of the pyrazolyl ring did not induce any appreciable shift of the emission wavelength (484 nm, **6**); however, the methyl group at the 3-position blue-shifted the emission by about 10 nm (474 nm, **5**). This is consistent with the results of

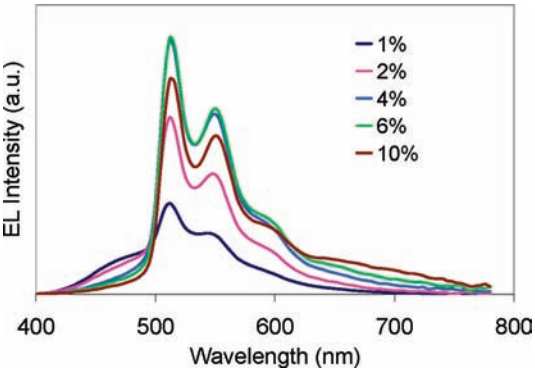

Figure 11. EL spectra of devices with various dopant concentrations in CBP host at the current density of 20 mA/cm^2.

DFT calculations, which showed significant contribution of the 3-carbon to the LUMO of the complexes. An electron donating group directly attached to this carbon would be expected to raise the LUMO energy. While complexes **3** and **5** showed poorly resolved emission at room temperature, all complexes **3**−**6** displayed better resolved spectra at 77 K (Figure 10). The main vibronic progression was in the range of 1136 to 1383 cm^{-1}. The emission spectra of **3**−**6** in pure solid state are shown in Supporting Information, Figure S10. Complexes **3** and **4** showed broad emissions, while **5** and **6** displayed resolved spectra. All spectra are red-shifted when compared with those in fluid state except for that of **5** where the first band is slightly blue-shifted. The red shift may be due to the intermolecular interaction in the solid state, although the excimer formation particularly in the case of **3** cannot be completely ruled out. The solvent effect on emission of **1** and **3** is moderate (7−8 nm hypsochromic shifts from toluene to acetonitrile) while the effect on emission of **4**−**6** is minimal (Supporting Information, Tables S2−S6). The concentration quenching was observed for complex **3** and **4** but not for **5** and **6**. The emission decay time of **3** (7.6 μs) at infinite dilution in 2-methyltetrahydrofuran is very similar to that of **1**. The emission lifetime of **4** at infinite dilution was estimated to be 4.9 μs. The quenching constant for both **3** and **4** was found to be the same, 8.0×10^8 M^{-1}sec^{-1}, which is smaller than those of **1** and **2**. The emission decay time for **5** and **6** were estimated to be 3.4 and 5.7 μs, respectively. The quantum yield and emission lifetime of **4**−**6** suggest a similar radiative decay rate to those of complexes **1** and **2**. This seems to be inconsistent with the DFT calculations that indicate a much smaller platinum contribution to the HOMOs of **3**−**6** (Supporting Information, Table S1). There could be several possible considerations. For example, the triplet emission might not be originated solely from the HOMO. It is interesting to note that the emissions of **4**−**6** occurred at higher energy than that of **1** even though **4**−**6** have smaller calculated HOMO−LUMO gaps. On the other hand, the energy gap between the lowest triplet state and the first singlet state might be smaller for the complexes **4**−**6**, which would indicate greater mixing of singlet character into the triplet state. However, as factors that affect radiative decay can be very complicated, a detailed time dependent DFT study in combination with a study of high resolution emission in a Shpol'skii matrix may be necessary to further elucidate the nature of the emissive transition states for these complexes.

Table 5. Performance Data of OLED Devices with 4% of **1** in TPBI-TCTA Host

current density (mA/cm2)	V [V]	L [cd/m^2]	η_c [cd/A]	EQE (%)	λmax (nm)	CIE (x, y)
0.01	3.31	5	50.0	14.7	512	0.318, 0.622
0.1	4.33	49	48.9	14.2	512	0.315, 0.623
1	5.92	455	45.5	13.1	512	0.316, 0.623
10	8.64	3698	37	10.6	512	0.316, 0.623

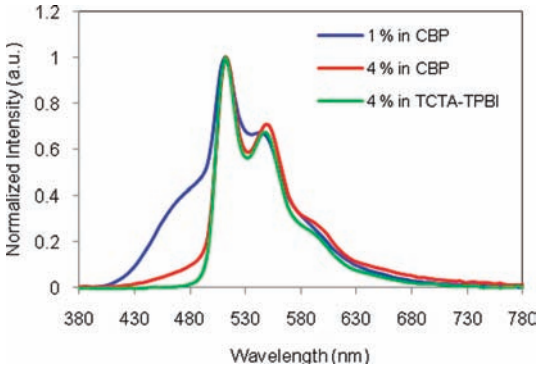

Figure 12. Comparison of EL spectra of Device with different structures (normalized at 512 nm).

OLED Application. Complex **1** was selected to demonstrate the utility of the highly emissive tetradentate cyclometalated platinum complexes as a phosphorescent emitter in OLED devices. Complex **1** has good thermal stability and could be sublimed without decomposition; therefore, it is suitable for fabricating OLED devices using vapor deposition technology. Complex **1** was first tested as a dopant in the CBP[34] host, a commonly used host for phosphorescent emitters. Different dopant concentrations were examined. The device structure is ITO/CF_x (1 nm)/ NBP (120 nm)/ CBP+ x wt % **1** (35 nm)/BAlq (10 nm)/Alq (40 nm)/Mg:Ag (220 nm). The performance of the devices was very poor. The maximum external quantum efficiency of about 2.2% was demonstrated by the device with 4% dopant concentration at 6 mA/cm^2. The low efficiency may be attributed to the unbalanced charge injection and the diffusion of excitons into the NPB layer. As can be seen from the electroluminescence spectra shown in Figure 11, an emission from the blue region (possibly emission from NPB) was presented and became more significant at lower dopant concentration. At higher dopant concentration, a broad emission at longer wavelength is growing, which may be due to the formation of excimer. However, at the concentration of 4% or less, the excimer emission is negligible.

To improve the performance of the device, a recently developed device configuration[35] with the use of mixed host and exciton blocking layer was employed to fabricate the devices. The devices have the following structure of layers: ITO/CF_x (1 nm)/ NBP (65 nm)/ TCTA (10 nm)/ (TPBI + 30 wt % TCTA)+ 4 wt % **1** (35 nm)/ TPBI (10 nm)/ Alq (40 nm)/ Mg:Ag (220 nm). NPB and Alq were used as hole and electron transporting layers, respectively. The use of the mixed host (TPBI and 30% wt % TCTA) is to facilitate the injection of both charges. A layer of TCTA (10 nm)

(34) Adachi, D.; Kwong, R. C.; Djurovich, P.; Adamovich, V.; Baldo, M. A.; Thompson, M. E.; Forrest, S. R. *Appl. Phys. Lett.* **2001**, *79*, 2082.
(35) Kondakova, M. E.; Pawlik, T. D.; Young, R. H.; Giesen, D. J.; Kondakov, D. Y.; Brown, C. T.; Deaton, J. C.; Lenhard, J. R.; Klubek, K. P. *J. Appl. Phys.* **2008**, *104*, 094501.

(4,4′,4″-*tris*(*N*-carbazolyl)triphenylamine) was used between hole transporting layer of NPB and the emissive layer to prevent triplet excitons from diffusing to the NPB layer. A thin layer of TPBI (2,2′,2″-(1,3,5-benzenetriyl)*tris*(1-phenyl-1-*H*-benzimidazole)) was used as the hole-blocking layer. All of these modifications are to confine the charge recombination. The performance of the devices was improved substantially, and the data are summarized in Table 5. The maximum efficiency of 14.7% was achieved at the current density of 0.01 mA/cm^2, which decreased gradually to 10.6% with the increase of the current density to 10 mA/cm^2. This is typical for a phosphorescent dopant and may be explained by the triplet−triplet annihilation that becomes more severe at higher current density.[36] The devices emitted bright green color with a maximum emission of 512 nm, which is almost identical to the emission in solution of 2-methyltetrahedrofuran. The color remains unchanged with the increase of current density. From the Figure 12, it can be seen that the emission in the blue region observed for the devices with CBP as host was completely eliminated in the modified device structure.

Conclusion

Six tetradentate bis-cyclometalated platinum complexes with general coordination patterns of (C^N*N^C)-Pt and (N^C*C^N)-Pt were synthesized, and their structures were confirmed by the X-ray crystal structure analysis. All complexes are emissive at room temperature in solution. Most of the complexes emitted with very high quantum yields, and some are among the highest reported for the platinum complexes. The complexes emitted in a wide spectral range from blue to red. The emissive states were characterized as primarily ligand-centered triplet states with MLCT admixture based on their photophysical properties including the absorption and emission spectra and lifetime of the emissive state. The ZFS of an emissive triplet state is characteristic of the degree of MLCT character in the transition[28] and was observed directly by high resolution spectroscopy for **1** in a Shpol'skii matrix. The ZFS found for **1** (23 cm^{-1}) was within the range of values found for bis(C^N)-cyclometalated Pt complexes such as Pt(ppy)$_2$ (32 cm^{-1}) and Pt(thpy)$_2$ (16 cm^{-1}) that have also been described as emitting from ^{3}LC states having significant admixture of MLCT character.[28,32a] In view of the similar nature of excited triplet states between **1** and Pt(ppy)$_2$, the high efficient room temperature emission from **1**, in contrast to the nonemissive nature of Pt(ppy)$_2$, may be mainly attributed to the rigidity of the tetradentate platinum complex. DFT calculations also suggested an ILCT characteristic of the excited states because of the localized characteristic of the HOMOs and LUMOs of the complexes. The application of the complexes in OLEDs was demonstrated by incorporating **1** into an emissive layer of an OLED using a mixed host and an exciton blocking layer. The devices demonstrated high performance with a maximum external efficiency of 14.7% and showed little evidence of excimer emission at moderate concentrations.

Experimental Section

Synthesis. General Procedures. All reactions involving moisture- and/or oxygen-sensitive organometallic complexes were carried out under nitrogen atmosphere and anhydrous conditions. Tetrahydrofuran (THF) and 2-methyltetrahydrofuran were distilled from sodium and benzophenone under nitrogen before use. All other anhydrous solvents were purchased from Aldrich Chemical Co. and were used as received. All other reagents were commercially available and used as received. Mass spectra were measured on a Waters ZMD mass spectrometer. Accurate mass measurements were made on a JEOL HX-110 mass spectrometer operated in Electron Impact (EI) ionization. NMR spectra were measured on a Mercury VX 300 or a Varian 500 spectrometer. Spectra were taken in $CDCl_3$ or CD_2Cl_2 using TMS as standard for ^{1}H NMR chemical shifts and the solvent peak ($CDCl_3$, 77.0 ppm; CD_2Cl_2, 53.8 ppm) as standard for ^{13}C NMR chemical shifts.

Preparation of *N*,*N*-di(2-bromopyrid-6-yl)aniline. To a 250 mL dry, nitrogen flashed flask were charged 2,6-dibromopyridine (11.85 g, 50 mmol), sodium *tert*-butoxide (4.8 g, 50 mmol), $Pd_2(dba)_3$ (0.366 g, 0.4 mmol), DPPF (0.443 g, 0.8 mmol), aniline (1.8 mL, 20 mmol), and anhydrous toluene (150 mL). The mixture was stirred at 80−90 °C overnight. After cooling to room temperature, the reaction mixture was poured into water, and the aqueous phase was extracted with ethyl acetate (EtOAc) (3 × 100 mL). The combined organic extracts were washed with water (200 mL) and brine (200 mL) and dried over $MgSO_4$. Filtration and evaporation produced dark brown oil, which was purified by chromatography on silica gel with a mixture of dichloromethane and heptane (v/v = 1:1) to provide a yellow solid, 4.83 g, 60%. ^{1}H NMR (300 MHz, $CDCl_3$) δ 7.3−7.45 (m, 4H), 7.28 (t, J = 7.2 Hz, 1H), 7.19 (d, J = 7.3, 2H), 7.09 (d, J = 7.6 Hz, 2H), 6.92 (d, J = 8.2 Hz, 2H). ^{13}C NMR (75 MHz, $CDCl_3$) δ 157.1, 143.4, 139.6, 139.4, 129.8, 127.9, 126.7, 122.0, 114.8. MS: m/z calcd 402.932; found 402.931.

Preparation of *N*,*N*-di(2-phenylpyrid-6-yl)aniline (L1). Representative Procedure. To a 250 mL flask were charged *N*,*N*-di-(2-bromopyrid-6-yl)aniline (2.44 g, 6 mmol), phenylboronic acid (2.18 g, 18 mmol), triphenylphosphine (0.314 g, 1.2 mmol), and ethylene glycol dimethyl ether (35 mL). A homogeneous solution was formed. To this solution was added 2 M K_2CO_3 (30 mL, 60 mmol). After the mixture was purged with nitrogen, $Pd(OAc)_2$ (0.067 g, 0.3 mmol) was added. The mixture was refluxed for 4 h and then cooled to room temperature. The reaction mixture was transferred into a separating funnel, and the organic layer was separated and retained. The aqueous phase was extracted with ethyl acetate (EtOAc) (3 × 50 mL). The combined organic layers were washed with water (100 mL) and brine (100 mL) and dried over $MgSO_4$. Filtration and evaporation produced a dark brown solid, which was purified by chromatography on silica gel with dichloromethane and heptane (v/v = 4:1) and recrystallization from heptane and dichloromethane to provide **L1** as white crystals, 1.66 g, 69%. ^{1}H NMR (500 MHz, CD_2Cl_2) δ 7.89 (d, J = 8 Hz, 4H,), 7.67 (t, J = 8 Hz, 2H,), 7.46 (d, J = 8 Hz, 2H), 7.45 (d, J = 8 Hz, 2H), 7.42−7.32 (m, 7H), 7.31 (t, J = 8 Hz, 2H), 7.07 (d, J = 8 Hz, 2H). ^{13}C NMR (125 MHz, CD_2Cl_2) δ 158.1, 155.9, 145.6, 139.7, 138.6, 129.9, 129.8, 129.1, 18.4, 127.1, 126.1, 115.7, 114.7. Anal. Calcd for $C_{28}H_{21}N_3$: C, 84.18; H, 5.30; N, 10.52; found: C, 84.21; H, 5.25; N, 10.47. MS: m/z calcd 399.1735; found 399.1731.

***N*,*N*-di(2-(2,4-difluorophenyl)pyrid-6-yl)aniline(L2).** Yield, 75%. ^{1}H NMR (500 MHz, $C_2D_2Cl_4$) δ 7.83(dt, $^4J_{H-F}$ = 8.8 Hz; J = 7.7 Hz, 2H), 7.73 (t, J = 7.8 Hz, 2H), 7.55 (d, J = 7.5 Hz, 2H), 7.5 (t, J = 7.5 Hz, 2H), 7.38 (d, J = 7.5 Hz, 2H), 7.35 (t, J = 7.5 Hz, H), 7.12 (d, J = 7.8 Hz, 2H), 6.98 (m, 2H), 6.94 (m, 2H). ^{13}C NMR (126 MHz, $C_2D_2Cl_4$,) δ 163.3, 161.3, 157.8, 150.7, 145.0, 138.6, 132.5, 129.9, 127.9, 126.1, 123.8, 118.8, 116.1, 112.2, 104.8. ^{19}F NMR (470 MHz, $C_2D_2Cl_4$, $CFCl_3$@ 0.00 pm) δ −109 (m, 1F), −110.9 (m, 1F). Anal. Calcd for $C_{28}H_{17}F_4N_3$: C, 71.33; H, 3.63; N, 8.91; found: C, 71.41; H, 3.58; N, 8.87. MS: m/z calcd 471.1359; found 471.1333.

Preparation of Platinum Complex (1). Representative Procedure. A mixture of the tetradentate C^N*N^C ligand **L1** (0.40 g,

(36) Adachi, D.; Baldo, M. A.; Forrest, S. R.; Thompson, M. E. *Appl. Phys. Lett.* **2000**, *77*, 904.

1 mmol), K_2PtCl_4 (0.42 g, 1 mmol), Bu_4NCl (few crystals), and glacial acetic acid (60 mL) was degassed and refluxed under nitrogen for 45 h. After cooling to room temperature, the yellow to orange precipitates were collected by filtration and washed with water and methanol, and dried in air. The crude materials were purified by flash chromatography on silica gel with dichloromethane as eluting solvent; the first yellow band was collected and evaporated to give 0.47 g of yellow crystals, 79%. ^{1}H NMR (500 MHz, CD_2Cl_2) δ 8.32 (m, J = 7.7 Hz, $^3J_{Pt-H}$ 25 Hz, 2H), 7.82 (d, J = 7.8 Hz, 2H), 7.75−7.68 (m, 4H), 7.67(t, J = 7.7 Hz, 1H), 7.64 (d, J = 7.8 Hz, 2H), 7.46 (d, J = 7.8 Hz, 2H), 7.41 (d, J = 7.3 Hz, 2H), 7.21 (t, J = 7.5 Hz, 2H), 6.51 (d, J = 8.7 Hz, 2H). ^{13}C NMR (125 MHz, CD_2Cl_2) δ 164.3, 149.6, 149.3, 147.7, 143.8, 137.4, 136.2, 132.2, 131.0, 130.3, 129.8, 124.4, 123.7, 114.7, 112.4. Anal. Calcd for $C_{28}H_{19}N_3Pt$: C, 56.76; H, 3.23; N, 7.09. Found: C, 56.63; H, 3.20; N, 7.06. MS: m/z calcd 592.1227; found 592.1240.

Complex (2). This complex was prepared using the same procedure, yielding the crude greenish yellow crystalline materials, 66%, which were purified by sublimation to give yellow needles, 57%. ^{1}H NMR (500 MHz, $C_2D_2Cl_4$) δ 8.07 (d, J = 8.0 Hz, 2H), 7.86 (t, J = 8.6 Hz, 2H), 7.8 (t, J = 7.3 Hz, 2H), 7.77 (m, 2H), 7.76 (m. 1H), 7.46 (d, J = 7.3 Hz, 2H), 6.79 (m, 2H), 6.59 (d, J = 8.6 Hz, 2H); ^{13}C NMR (126 MHz, $C_2D_2Cl_4$) δ 138.3, 132.1, 130.3, 130.2, 117.6, 116.3, 114.3, 99.9 (because of very poor solubility, only partial carbon signals were observed); ^{19}F NMR (470 MHz, $C_2D_2Cl_4$, $CFCl_3$@ 0.00 pm) δ −107.4 (m, 2F), −109.1 (m, 2F). Anal. Calcd for $C_{28}H_{15}F_4N_3Pt$: C, 50.61; H, 2.28; N, 6.32. Found: C, 50.53; H, 2.35; N, 6.32. MS: m/z calcd 664.0852; found 664.0873.

***N*,*N*-di(3-bromophenyl)aniline.** To a 100 mL dry, nitrogen flushed flask was charged with aniline (186 mg, 2 mmol), dibromobenzene (1.40 g, 6 mmol), sodium *tert*-butoxide (576 mg, 6 mmol), $Pd(dba)_2$ (92 mg, 0.16 mmol), DPPF (89 mg, 0.16 mmol) in toluene (10 mL). The reaction mixture was refluxed overnight. After cooling to room temperature, 20 mL of ethyl acetate was added and stirred for a while. The precipitate formed was filtered, and the filtrate was evaporated. The crude mixture was purified by chromatography on silica gel with a mixture of hexane and ethyl acetate (v/v = 15:1) to give a white solid, 182 mg, yield 45%. ^{1}H NMR (300 MHz, $CDCl_3$), δ 7.4−6.8 (m, 13 H). ^{13}C NMR (75 MHz, $CDCl_3$), δ 148.7, 146.6, 130.5, 129.6, 126.5, 125.9, 125.1, 124.2, 122.9, 122.3. Anal. Calcd for $C_{18}H_{13}Br_2N$: C, 53.63; H, 3.25; N, 3.47. Found: C, 53.79; H, 3.16; N, 3.44.

***N*,*N*-di(3-(pyridin-2-yl)phenyl)aniline (L3).** To a 250 mL, 3 necked dry, nitrogen flushed flask was charged with *n*-BuLi (1.6 M in hexanes, 6 mL, 9.6 mmol) and cooled to −78 °C. To this, a solution of 2-bromopyridine (0.8 mL, 8 mmol) in 7 mL of ether was added dropwise. After stirring for 30 min, the reaction mixture was warmed to 0 °C, and zinc chloride solution (1.0 M in diethyl ether, 8 mL, 8 mmol) was added dropwise. The mixture was then warmed to room temperature. *N*,*N*-di(3-bromophenyl)-aniline (800 mg, 2 mmol), $Pd(PPh_3)_4$ (230 mg, 0.2 mmol), and 8 mL of diethyl ether were added, and the reaction mixture was refluxed for 36 h. After cooling, the reaction mixture was quenched by water and extracted with ethyl acetate (3 × 75 mL). The combined organic phases were washed with water (100 mL), brine (100 mL), dried over $MgSO_4$, filtered, and evaporated. The crude product was purified by chromatography on silica gel with a mixture of petroleum ether and ethyl acetate (v/v = 2:1) to give a solid, 597 mg, yield 75%. ^{1}H NMR (500 MHz, CD_2Cl_2), δ 8.61 (d, J = 4.0 Hz, 2H), 7.77 (s, 2H), 7.66−7.63 (m, 4H), 7.60−7.54 (m, 2H), 7.35 (t, J = 7.5 Hz, 2H), 7.25 (t, J = 7.5 Hz, 2H), 7.20−7.14 (m, 6H), 7.00 (t, J = 7.0 Hz, 1H). ^{13}C NMR (75 MHz, $CDCl_3$), δ 157.2, 149.6, 148.3, 147.8, 140.8, 136.7, 129.7, 129.3, 125.0, 124.1, 122.8, 122.73, 122.1, 121.6, 120.7. Anal. Calcd for $C_{28}H_{21}N_3$: C, 84.18; H, 5.30; N, 10.52; found: C, 84.11; H, 5.18; N, 10.45.

Complex (3). This complex was prepared following the general procedure described for complex **1**. Yield 30.5%. ^{1}H NMR (500 MHz, CD_2Cl_2) δ 8.97 (d, J = 5.5 Hz, 2H), 8.01 (s, 1H), 7.99 (s, 1H), 7.94 (td, J = 7.5, 1.5 Hz, 2H), 7.66 (t, J = 7.5 Hz, 2H), 7.53 (tt, J = 7.5, 1.5 Hz, 1H), 7.45−7.42 (m, 2H), 7.34 (d, J = 7.5 Hz, 2H), 7.34−7.32 (m, 2H), 7.00 (t, J = 7.5 Hz, 2H), 6.28 (d, J = 8.5, 2H). ^{13}C NMR (125 MHz, CD_2Cl_2) δ 166.6, 147.9, 146.7, 145.8, 142.7, 138.5, 131.8, 131.2, 128.6, 128.0, 123.5, 122.6, 120.0, 118.9, 116.2. MS m/z 592; Anal. Calcd for $C_{28}H_{19}N_3Pt \cdot 1/3(CH_2Cl_2)$: C, 54.81; H, 3.19; N, 6.77. Found: C, 54.95; H, 3.10; N, 6.76.

Preparation of *N*,*N*-di(3-(1*H*-pyrazol-1-yl)phenyl)aniline L4. General Procedure. To a 25 mL dry, nitrogen flushed flask were charged *N*,*N*-di(3-bromophenyl)aniline (200 mg, 0.5 mmol,), pyrazole (101 mg, 1.5 mmol), potassium carbonate (150 mg, 1.1 mmol), copper iodide (17 mg, 0.1 mmol), trans-*N*,*N*′-dimethylcyclohexanediamine (66 μL, 0.4 mmol), and toluene (5 mL). The mixture was refluxed for 5 days. After cooling to room temperature, 20 mL of ethyl acetate was added, and the precipitate formed was filtered out. The filtrate was concentrated, and the product was separated by column chromatography with hexane and ethyl acetate (v/v = 5:1) to give a solid of 301 mg, yield 80%. ^{1}H NMR (500 MHz, CD_2Cl_2) δ 7.86 (d, J = 2.5 Hz, 2H), 7.62 (d, J = 2.0 Hz, 2H), 7.47 (t, J = 2.5 Hz, 2H), 7.38−7.30 (m, 6H), 7.20−7.15 (m, 2H), 7.10 (tt, J = 8.0, 1.0 Hz, 1H), 7.04−6.98 (m, 2H), 6.40 (t, J = 2.5 Hz, 2H). ^{13}C NMR (75 MHz, $CDCl_3$) δ 148.7, 147.0, 141.3, 141.0, 130.2, 129.6, 126.9, 124.9, 123.8, 122.0, 114.8, 113.8, 107.5. Anal. Calcd for $C_{24}H_{19}N_5$: C, 76.37; H, 5.07; N, 18.55. Found: C, 76.09; H. 4.94; N, 18.44.

***N*,*N*-di(3-(3-methyl-1*H*-pyrazol-1-yl)phenyl)aniline (L5).** Yield 68%. ^{1}H NMR (500 MHz, CD_2Cl_2) δ 7.74 (d, J = 2.5 Hz, 2H), 7.43 (t, J = 2 Hz, 2H), 7.36−7.28 (m, 6H), 7.15 (d, J = 6.5 Hz, 2H), 7.09 (tt, J = 7.5, 1.5 Hz, 1H), 6.96 (t, J = 2.5 Hz, 1 H), 6.94 (t, J = 2.0 Hz, 1H), 6.20 (d, J = 2.5 Hz, 2H), 2.27 (s, 6H). ^{13}C NMR (75 MHz, $CDCl_3$) δ 150.5, 148.6, 147.1, 141.3, 130.2, 129.5, 127.5, 124.7, 123.5, 121.7, 114.5, 113.6, 107.5, 13.7. Anal. Calcd for $C_{26}H_{23}N_5$: C, 77.01; H, 5.72; N, 17.27. Found: C, 76.61; H, 5.58; N, 16.96.

***N*,*N*-di(3-(4-methyl-1*H*-pyrazol-1-yl)phenyl)aniline (L6).** Yield 85%. ^{1}H NMR (500 MHz, CD_2Cl_2) δ 7.65 (s, 2H), 7.48−7.42 (m, 4H), 7.36−7.28 (m, 6H), 7.18 (d, J = 7.5 Hz, 2H), 7.13 (t, J = 7 Hz, 1H), 6.88 (d, J = 6.5 Hz, 2H), 2.12 (s, 6H). ^{13}C NMR (75 MHz, $CDCl_3$) δ 148.6, 147.1, 141.7, 141.3, 130.2, 129.5, 125.5, 124.8, 123.6, 121.6, 118.2, 114.3, 113.3, 8.9. Anal. Calcd for $C_{26}H_{23}N_5$: C, 77.01; H, 5.72; N, 17.27. Found: C, 77.22; H, 5.80; 17.29.

Complex 4. Following general procedure, this complex was prepared in 25% yield. ^{1}H NMR (500 MHz, CD_2Cl_2) δ 8.10 (d, J = 3.0 Hz, 2H), 7.89 (d, J = 1.5 Hz, 2H), 7.66 (t, J = 8.0 Hz, 2H), 7.53 (tt, J = 7.0, 1.0 Hz, 1H), 7.31 (d, J = 7.5 Hz, 2H), 6.96−6.88 (m, 4H), 6.64 (t, J = 2.5 Hz, 2H), 6.04 (dd, J = 8.0, 2.0 Hz, $^3J_{Pt-H}$ 17 Hz, 2H). ^{13}C NMR (75 MHz, CD_2Cl_2) δ 146.2, 145.3, 143.4, 139.7, 131.7, 131.3, 128.2, 127.1, 123.6, 115.6, 114.9, 107.5, 103.5. MS m/z 570.11 (M^+); Anal. Calcd for $C_{24}H_{17}N_5Pt$: C, 50.53; H, 3.00; N, 12.28. Found: C, 50.33; H, 2.88; N, 12.24.

Complex 5. Following general procedure, this complex was prepared in 33% yield. ^{1}H NMR (500 MHz, CD_2Cl_2) δ 8.01 (d, J = 3.0 Hz, 2H), 7.63 (tt, J = 8.0, 1.5 Hz, 2H), 7.5 (tt, J = 7.5 Hz, 1H), 7.26 (dt, J = 7.0, 1.0 Hz, 2H), 6.92−6.84 (m, 4H), 6.42 (d, J = 2.5 Hz, 2H), 5.97 (dd, J = 7.5, 2.0 Hz, 2H), 2.54 (s, 6H). ^{13}C NMR (75 MHz, CD_2Cl_2) δ 151.3, 146.7, 145.4, 142.9, 131.7, 131.2, 129.6, 128.0, 123.5, 114.2, 113.8, 107.9, 102.4, 16.1. MS m/z 598.14(M^+); Anal. Calcd for $C_{26}H_{21}N_5Pt$: C, 52.17; H, 3.54; N, 11.70. Found: C, 52.15; H, 3.48; N, 11.63.

Complex 6. Following general procedure, this complex was prepared in 25% yield. ^{1}H NMR (500 MHz, CD_2Cl_2) δ 7.88 (s, 2H), 7.69 (s, 2H), 7.64 (t, J = 8.0 Hz, 2H), 7.51 (tt, J = 7.0, 1.5 Hz, 1H), 7.29 (d, J = 7.5 Hz, 2H), 6.90−6.82 (m, 4H), 5.99 (dd, J = 7.0, 1.0 Hz, $^3J_{Pt-H}$ 17 Hz, 2H), 2.24 (s, 6H). ^{13}C NMR

(75 MHz, CD_2Cl_2) δ 146.5, 145.3, 143.3, 139.8, 131.7, 131.2, 128.0, 125.8, 123.4, 118.2, 115.6, 114.5, 103.2, 9.4. MS m/z 598.14(M^+); Anal. Calcd for $C_{26}H_{21}N_5Pt$: C, 52.17; H, 3.54; N, 11.70. Found: C, 51.71; H, 3.45; N, 11.49.

Photophysical Experiments. Absorption spectra were recorded using a HP-8453 or Varian dispersive spectrometer (Cary 5E) diode array UV/vis spectrophotometer, using 1 cm path-length quartz cuvettes. A 10 cm path length quartz cuvette was used for recording the weak lowest energy absorption spectra of **1** and **2**. The steady state emission spectra were measured using a PTI QM-4CW system.

Quantum yields were measured using comparative method at room temperature in a 2-methyltetrahydrofuran solution. The solution was deoxygenated by purging with nitrogen gas for 20 min. A long necked 1 cm quartz cuvette was used for measurements. The cuvette was cooled with a dry ice-acetone bath to prevent solvent loss. A solution of quinine sulfate dihydrate in 0.1 N H_2SO_4 was used as a reference. The optical density of both sample and reference solutions was maintained below 0.1 AU at the excitation wavelength. Phosphorescence lifetime measurements were performed on the same fluorimeter equipped with variable high rep rate pulsed xenon source for excitation and were limited to lifetimes $> 0.4\,\mu$s. Samples of compound **1** in a Shpol'skii matrix of *n*-octane for high resolution spectroscopy were prepared as previously described.[37] Time-resolved measurements for complexes **1** and **2** were carried out at a variety of wavelengths (sample dependent) on the Low Temperature Photo-Luminescence (LTPL) instrument. The LTPL setup consisted of an ISA monochromator (model 750M) for the emission monochromator, a variety of optical lenses and filters, and a PMT with associated electronics. The excitation source was a Continuum Minilite Nd:YAG laser excitation (3−5 ns pulse width at 355 nm, ≈3 mJ per pulse). The RCA PMT detects emission decays after each flash at a given wavelength as selected by the 750 M monochromator. The decays are averaged using a Tektronix digital oscilloscope (model TDS 3032) and acquired by computer. Normal decay curves are the average of 256 events (flashes).

X-ray Crystallography. Crystals were grown by diffusing hexanes to a dichloromethane solution of the complexes. A crystal was selected and mounted on a glass fiber. All measurements were made using graphite-monochromated Cu Kα radiation (1.54178 Å) on a Bruker-AXS three-circle diffractometer, equipped with a SMART Apex II CCD detector. In each case, initial space group determination was based on a matrix consisting of 120 frames. The data were reduced using SAINT+,[38a] and empirical absorption correction was applied using SADABS.[38b] Structures were solved using direct methods. Least-squares refinement for all structures was carried out on F^2. All non-hydrogen atoms were refined anisotropically, except for the solvent CH_2Cl_2 carbon in **3**. In the case of **3**, three significant (> 2 e/Å^3) peaks were present; however, each was very close to a platinum atom. Platon[39] detected a void having a volume of 232.0 Å^3 in the unit cell of **3**. However, no additional solvent molecule was found in the difference map. Platon Squeeze was not found to significantly improve the structure, so the non-Squeeze results were used. Hydrogen atoms were placed in calculated positions and allowed to be refined isotropically as riding models. Structure solutions, refinement, and the calculation of derived results were performed using the SHELXTL package of computer programs.[40] Details of the X-ray experiments and crystal data are summarized in Table 1.

OLED Fabrication. Bottom-emitting OLEDs, were fabricated on ∼1.1-mm thick glass substrates precoated with a transparent indium tin oxide (ITO) conductive layer having a thickness of ∼22 nm and a sheet resistance of ∼68 X/square. The substrates were cleaned and dried using a commercial glass scrubber tool. The ITO surface was subsequently treated with oxygen plasma, and then conditioned as a modified anode by decomposing CHF_3 gas in a plasma treatment chamber to deposit an ∼1 nm-thick layer of CFx. Six substrates in each experiment were then transferred into a vacuum chamber for sequential deposition of all organic and metal layers on top of the substrates by a thermal evaporation method without breaking vacuum ($\sim 10^{-6}$ Torr). The deposition rates and doping concentrations of materials were controlled and measured in situ using calibrated thickness monitors. The deposition rate of the organic host materials was ∼0.4 nm/s, and the deposition rates of the dopant materials were adjusted according to the volume ratio in the host materials. The Al cathode formed on top of the organic layers has a thickness of about 210 nm. Each OLED has an emission area of 1 mm^2. The devices were transferred from the vacuum chamber into a nitrogen-filled glovebox for encapsulation before testing. The EL characteristics of all the fabricated devices were evaluated using a constant current source (Keithley 2400 SourceMeter) and a photometer (Photo Research SpectraScan PR 650) at room temperature. The external quantum efficiencies (EQE) of the devices were calculated with the assumption of a Lambertian angular distribution of light emitted from the devices.

Acknowledgment. We thank Robert Schultz and Thomas Marchincin for part of photophysical measurements and Dr. Denis Kondakov for helpful discussion of photophyiscal experiments. We also thank Dr. Thomas Jackson for HRMS measurements and Dr. William C. Lenhart for part of NMR measurements. Financial support from the Research Corporation for Science Advancement (SH), Burroughs Wellcome Fellowship (D.A.K.V.), and East Carolina University is gratefully acknowledged. R.D.P. acknowledges NSF (CHE-0443345) and the College of William and Mary for the purchase of the X-ray equipment.

Supporting Information Available: Crystallographic data in CIF format for **1**, **3**, and **5**. Experimental molecular geometries for **1**, **3**, and **5** and DFT calculated geometries for **4**−**6**. Calculated energies and Pt character of molecular orbitals. Stern−Volmer plots, excitation spectra of **1** and **2**, solid state emission spectra of **1**−**6**, and solvent effects. This material is available free of charge via the Internet at http://pubs.acs.org.

(37) Marchetti, A. P.; Deaton, J. C.; Young, R. Y. *J. Phys. Chem. A* **2006**, *110*, 9828–9838.

(38) (a) *SAINT PLUS*; Bruker Analytical X-ray Systems: Madison, WI, 2001. (b) *SADABS*; Bruker Analytical X-ray Systems: Madison, WI, 2001.

(39) Spek, A. L. *J. Appl. Crystallogr.* **2002**, *36*, 7.

(40) Sheldrick, G. M. *Acta Crystallogr., Sect. A* **2008**, *64*, 112.